NUCLEAR ENGINEERING AND DESIGN 35 (1975) 1-12. © NORTH-HOLLAND PUBLISHING COMPANY

# A POROUS BODY MODEL FOR PREDICTING TEMPERATURE DISTRIBUTION IN WIRE-WRAPPED FUEL ROD ASSEMBLIES

E.U. KHAN, W.M. ROHSENOW, A.A. SONIN and N.E. TODREAS

*Departments of Mechanical and Nuclear Engineering, Massachusetts Institute of Technology, Cambridge, Massachusetts 02139, USA*

Received 6 June 1975

A porous body model, new in its application for predicting temperature distributions in wire-wrapped fuel rod assemblies, has been developed. The model developed for thermal transport in wire-wrapped rod bundles is similar in principle to the one which has long been successfully used for heat transfer in fixed beds of packed solids. Although the model is applicable to bundles in forced and mixed (combined forced and free) convection, attention in this paper is confined to bundles operating in forced (negligible natural) convection only. The results obtained from this analysis were found to predict available data with as good a precision as does the more complex analysis.

## 1. Introduction

In liquid metal fast breeder reactors (LMFBRs), the fuel and blanket assemblies are subject to severe radial gradients in the rate of heat generation and have a wide range of flow conditions. Core designers have evolved a number of numerical methods for predicting temperature and pressure distributions within these assemblies in order to determine cladding hot spots, assembly housing bowing and deformation, and the points of incipient boiling and voiding.

In most existing calculation procedures [2–9], the reactor assembly is divided into a large number of subchannels (the space between three adjacent rods in a LMFBR is generally used to define a subchannel). A different method is introduced in ref. [1], where the rod array in an LMFBR fuel assembly is divided into only two regions, each of which is treated as a continuum by viewing the wire-wrapped bundle as a porous body. The two-region model approach was also used in ref. [2] but the calculational nodes were still identified with locations of the subchannel centroids. In this paper we extend and clarify the method introduced in ref. [1]. The key accomplishment of this paper is the description of the complex thermal-hydraulic phenomena in a wire-wrapped LMFBR assembly in terms of a relatively simple model whose solution requires little computational time. The results obtained from this analysis were found to predict available data with as good a precision as do the results from the more complex methods of analysis.

This paper deals only with assemblies which operate under conditions of forced convection with negligible effects of natural convection. This restriction will be further discussed and relaxed in a subsequent paper.

## 2. Proposed model

A typical LMFBR fuel assembly consists of 217 fuel rods arranged in a hexagonal array with uniform spacing maintained between the rods by wire wraps. A typical blanket assembly consists of 61 fuel rods of considerably different geometrical dimensions but also spaced by one wire wrap around each rod. There are two major hydrodynamic effects of the presence of wire wraps on the fuel assembly design. Its presence increases the pressure drop and thus the pumping power required, but has the virtue of enhancing flow mixing in the bundle and thereby reducing temperature gradients if they exist. The fuel assemblies always operate at a high

Reynolds number (50–70 x $10^3$) during the steady-state operation of an LMFBR while the Reynolds number in the blanket assemblies may be in the laminar, transition or turbulent flow regime. Thus, fuel assemblies usually operate in the region where free convection is negligible as compared to forced convection, whereas the blanket assemblies may operate in the region where free convection is of the same magnitude as forced convection and also in the region where free convection may be much smaller than forced convection. The term mixed convection is used here to specify the regime where natural (free) and forced convection effects are both important and the term 'forced convection' implies that natural convection effects are negligibly small.

Among the various modes of energy transport that exist in the steady-state operation of an LMFBR rod assembly in forced convection, energy redistribution by thermal conduction through the fluid and by convective 'lateral mixing' caused by the presence of wire wraps are the predominant modes. Heat transfer by conduction through the individual fuel rods and by conduction through contacts between fuel rods (where wire-wrap spacers cross the gap between fuel rods) is small and is neglected.

The wire-wrapped rods are packed in an array which is enclosed by a housing, and as a result there is a region of flow next to the housing wall which is quite different in character from the flow in the central region. In the central core the mean flow oscillates around each rod as it progresses in an axial direction. This oscillation of flow, shown in fig. 1, may be imagined to contribute an effective eddy diffusivity superimposed on the normal eddy diffusivity associated with turbulence. Thus, a basis of our model is the existence of a uniform lateral enhanced eddy diffusivity $\epsilon$ for heat transfer in the inner region of the bundle. The eddy diffusivity in the axial direction is not significantly enhanced by the presence of wire wraps. In the outer region near the wall the flow field is quite different. Since the wire wrap is spiralled around each rod in the same direction, the flow progresses with both an axial component and a tangential component parallel to the wall.

The proposed model imagines the existence of a large number of closely spaced rods, and treats the rod assembly as a porous medium, approximating it as a continuum. The difference in the flow pattern in the outer and inner regions of the assembly suggests that the bundle be divided into two regions; an inner core surrounded by an outer region close to the housing wall. The energy generation by the rods is modeled by a continuous volumetric heat source distribution $Q(x, y, z)$, which simulates heat generation in the real rods. The energy transfer in the transverse direction is modeled by an effective eddy diffusivity, which includes the fluid oscillations due to the presence of wire wraps and also any other means of energy transport, such as natural turbulence. This present model is similar in principle to the one which has been used to study heat and mass transfer in porous media [10–13]. The

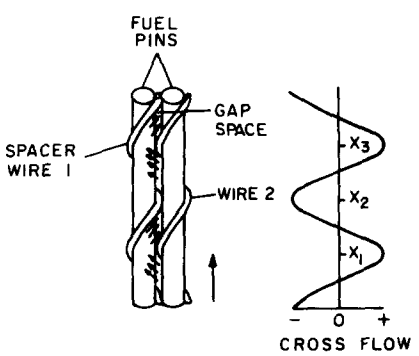


Fig. 1. Transverse flow distributions through gap spaces.

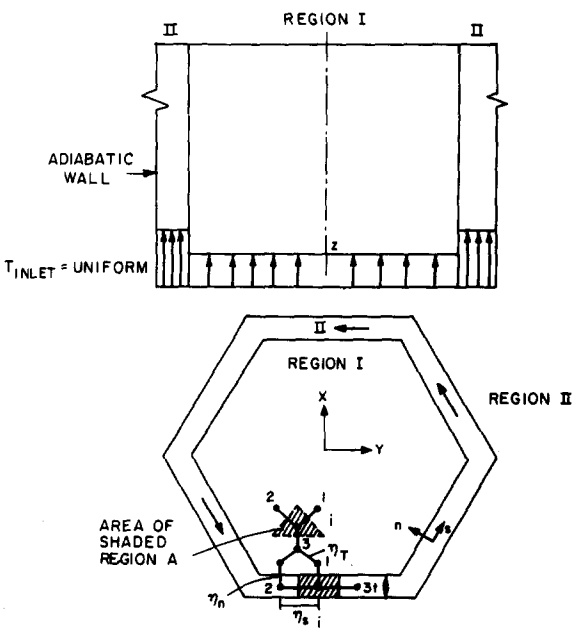


Fig. 2. Cross-section of a model showing location of nodes.

packed bed is analogous to the bundle of rods in the present case.

In what follows the inner region will be region I and is assumed to have a uniform superficial axial velocity $(U_I)_z$ (i.e. uniform volumetric flow rate per unit total area). The outer region, with a peripheral velocity component, is region II. It is assumed to have a uniform superficial axial velocity $(U_{II})_z$ and a uniform circumferential velocity $(U)_s$. The distance from the housing wall at which the circumferential (swirl) velocity becomes negligibly small must determine the thickness $t$ of the outer region.

The energy transport equation for region I may be written (fig. 2)

$$\rho C_p (U_I)_z \frac{\partial T}{\partial z} = (\rho C_p \epsilon_I + \kappa K)\left(\frac{\partial^2 T}{\partial x^2} + \frac{\partial^2 T}{\partial y^2}\right) + Q(x, y, z). \tag{1}$$

The coefficient $\kappa$ which multiplies the thermal conductivity accounts for the distortion of heat flow lines as they curve around the rods which do not transmit heat. This is further discussed in the next section.

In region II the energy transport equation is

$$\rho C_p (U)_s \frac{\partial T}{\partial s} + \rho C_p (U_{II})_z \frac{\partial T}{\partial z} = (\rho C_p \epsilon_n + \kappa K)\frac{\partial^2 T}{\partial n^2} + (\rho C_p \epsilon_s + \kappa K)\frac{\partial^2 T}{\partial s^2} + Q(s, n, z). \tag{2}$$

Axial conduction has been neglected. On the right-hand side of eq. (2) the second term (which represents energy transport in the $s$ direction, parallel to the duct wall, by conduction and by eddy diffusivity) can be shown to be an order of magnitude smaller than the first term on the left-hand side (which represents energy transport by convection in the $s$ direction). However, it has been retained in this analysis for completeness. Since in region II the convection effects will turn out to be more important than the energy transport due to mixing, the value of $\epsilon$ parallel to the duct wall may be assumed equal to its value in region I without any significant difference in result. The magnitude of $\epsilon$ in region II perpendicular to the wall is also taken equal to $\epsilon$ in region I, for the sake of simplicity. This was later justified by an excellent comparison of predictions with data.

The boundary conditions coupling eqs (1) and (2) require that the fluid temperature and the heat flux be continuous across the boundary between the two regions. The fluid temperature distribution at $z = 0$ and the thermal boundary condition at the container wall must be specified. In what follows, the bounding wall is assumed to be insulated.

Equations (1) and (2) may be written in a dimensionless form as follows:

*region I*

$$\frac{(U_I)_z}{\bar{U}} \frac{\partial h^*}{\partial z^*} = (\epsilon^* + \kappa\alpha^*)\left(\frac{\partial^2 h^*}{\partial x^{*2}} + \frac{\partial^2 h^*}{\partial y^{*2}}\right) + Q^*(x^*, y^*, z^*), \tag{3}$$

*region II*

$$C\frac{\partial h^*}{\partial s^*} + \frac{(U_{II})_z}{\bar{U}}\frac{\partial h^*}{\partial z^*} = (\epsilon^* + \kappa\alpha^*)\frac{\partial^2 h^*}{\partial s^{*2}} + (\epsilon^* + \kappa\alpha^*)\frac{\partial^2 h^*}{\partial n^{*2}} + Q^*(s^*, n^*, z^*), \tag{4}$$

where

$C = U_s/\bar{U}$ = swirl velocity ratio in region II;

$h^* = \rho C_p \bar{U}[T(x, y, z) - T_{IN}]/(\bar{Q} d_e)$ region I;

$h^* = \rho C_p \bar{U}[T(s, n, z) - T_{IN}]/(\bar{Q} d_e)$ region II;

$\alpha^* = \alpha/(\bar{U} d_e)$; $\epsilon^* = \epsilon/(\bar{U} d_e)$; $z^* = z/d_e$;

$s^* = s/d_e$; and $n^* = n/d_e$.

Along with the boundary conditions described earlier, eqs (3) and (4) may be solved in a differential form or in a finite difference form.

## 3. Solution of the equations

Based on the equations one expects $h^*$ to be a function of

$$h^* = h^*\underbrace{(x^*, y^*, z^*}_{\text{indep. variables}}; \underbrace{\epsilon^*, C, \kappa\alpha^*, (U_I)_z/\bar{U}, (U_{II})_z/\bar{U}, t^*}_{\text{parameters}}) \tag{5}$$

where $t^*$ is the dimensionless thickness of region II defined below.

One can determine $h^*$ for any given problem provided the geometry is known, and the boundary conditions at the wall and distribution of $Q^*(x^*, y^*, z^*)$ are stated. For a specific problem one can determine

the following from external considerations as discussed below: (a) $(U_I)_z/\bar{U}$, $(U_{II})_z/\bar{U}$;(b) $\kappa$; and (c) $t^*$.

(a) For a particular total flow rate the magnitudes of $(U_I)_z/\bar{U}$ and $(U_{II})_z/\bar{U}$ are determined from the hydraulic diameter flow analysis of Novendstern [16] and from experimental data [14, 15, 20]. At present, there is a small difference in the analytically and experimentally determined values of these velocities [17]. The experimental data show that the average axial velocity, over a spacer pitch, is nearly uniform in the entire bundle. The hydraulic diameter flow split shows that the wall region has a slightly higher velocity than the central region. In view of this uncertainty, a range of values $(\bar{U}_I)_z/\bar{U}$ and $(\bar{U}_{II})_z/\bar{U}$, spreading from the experimental to the analytical predictions, was used to determine temperature distributions. It was found that the effect of this range in flow split on exit temperature distributions of an LMFBR fuel bundle is very small [17].

(b) The presence of $\kappa$ in the equations may be explained as follows. In the present model the heat transferred from one point to another, at a given plane, would be over-predicted because it is assumed that there are no rods within the hexagonal duct. In actuality the presence of the rods considerably distorts the heat flow path. The heat flow lines must curve around the rods, which results in an increase in the length of their path. This is commonly termed 'tortuosity' [19] in the literature. To take into account the effect of tortuosity in our model, the molecular conductivity term was multiplied by the coefficient $\kappa$ (obviously $\kappa \leqslant 1$). Although tortuosity also affects eddy diffusivity in a similar manner as it does conductivity we chose to include this effect in the definition of $\epsilon^*$ because $\epsilon^*$ is determined empirically from data. The presence or absence of the coefficient $\kappa$ with $\epsilon^*$ would only change the magnitude of $\epsilon^*$ without changing the end result.

In principle the value of $\kappa$ can be determined for any given geometry of the fuel bundle by solving the heat conduction equation $\nabla^2 T = 0$ for the configuration shown in fig. 3. It was observed that, for all sets of forced connection data analysed, the eddy diffusivity term $\epsilon^*$ was at least an order of magnitude larger than $\kappa\alpha^*$. $\kappa$ was found to be nearly equal to the minimum lateral porosity $\lambda_L$ of the rod bundle, i.e. $\lambda_L = [1-(d/p)]$, where $p$ is the center-to-center distance between rods.

(c) The difference in flow field between the inner core of an assembly and the wall region suggests that the bundle be divided into two regions (fig. 4). The distance from the housing wall at which the (swirl velocity becomes negligibly small must determine the thickness $t$ of the outer region. It is intuitively expected that the swirl flow becomes very small in the vicinity of the gap between the peripheral rods, i.e. those adjacent to the housing wall. Therefore, the distance between the wall and a position close to the gap between peripheral rods should determine $t$. In the present study $t$ ($t^* = t/d_e$) is taken equal to the perpendicular distance between the wall and the line joining the centers of the peripheral rods.

From dimensional considerations, $\epsilon^*$ and $C$, the remaining quantities, are functions of the following quantities:

$$\epsilon^* = \epsilon^*(p/d, h/d, Re, Pr), \tag{6}$$

$$C = C(p/d, h/d, Re, Pr). \tag{7}$$

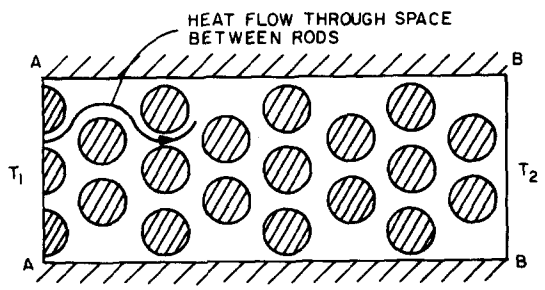


Fig. 3. Two-dimensional thermal field modeled as one-dimensional with use of coefficient $K$, where AA = isotherm at temperature $T_1$ and BB = isotherm at temperature $T_2$.

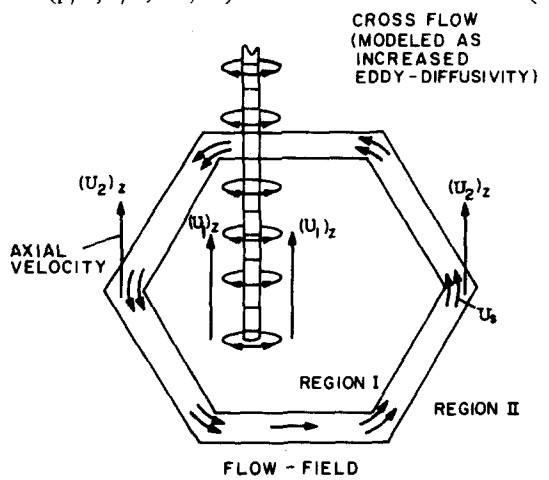


Fig. 4. Flow fields in the two regions.

Since these functions are unknown, we proceed by matching data to obtain them, then check whether we can predict any data within the range of applicability of these functions.

Equations (3) and (4) are solved in a finite difference form. A forward difference scheme is used in the axial direction. The hexagonal shape of the boundary walls suggests an equilateral triangular grid, as drawn in fig. 2, with equal lengths $\eta_T^*$ between nodes. The mesh size $\eta_T^*$ can be of any convenient size. Unlike in subchannel analysis methods [2–9] the spacing between nodes does not have to be taken equal to the distance between the centroids of the subchannels, but it may be so taken. In region II it is possible to use more than one node in a direction perpendicular to the wall. Thus two-dimensional temperature gradients in the wall region II can be obtained. The details of the numerical scheme and the stability criteria are developed in ref. [29].

The resulting computer program was given the name ENERGY-I. The magnitudes of $\epsilon^*$ and $C$ were established by assuming various magnitudes and selecting those which produced fluid temperature distributions in agreement with available test data. The program requires about 20 sec running time on an IBM-360 to determine the fluid temperature at all axial positions of a prototype 217 pin LMFBR bundle. Because the modeling of the wire wrap provides additional eddy diffusivity, the temperature distributions within the initial axial region between $z = 0$ and $z = h$ ($h$ = wire wrap axial pitch) are not expected to match experimental data to the same degree of accuracy as the data downstream of the first wire pitch.

## 4. Evaluation of $\epsilon^*$ and $C$ from data analysis

Tables 1 and 2 list the available data useful for determining $\epsilon^*$ and $C$ for fuel assemblies. The data are listed in table 1 according to bundle size and in table 2 according to typical characteristic geometrical parameters found in the literature. Several types of experiments, listed in table 1, have been used, e.g. electrolyte injection and conductivity probe measurements, hot water injection and heat pin experiments. The procedure for determining $\epsilon^*$ and $C$ from a typical set of data, the ORNL FFM-2A experiment [21], will be described.

Figure 5 shows a cross section of the 19-rod ORNL bundle along with the important parameters of the ORNL study. The heated length of the pins was 21 in. The axial power profile was uniform. Liquid sodium

Table 1.
List of data analysed based on bundle size. 1 1, 2, . . ., 11 number assigned to each experiment for use in Table 2. 2 Type of experiment: (a) hot water injection; (b) salt injection; (c) heated pin; and (d) laser.

| Ref. | No. of pins | | | | | | | Refs. |
|---|---|---|---|---|---|---|---|---|
| | 7 | 19 | 37 | 61 | 91 | 127 | 217 | |
| ANL–RAS | | | | | 8 (a) | | | [15] |
| ANL–CT | | | | | 9 (b) | | | [14] |
| ANL–CT | 1 (b) | | | | | | | [27] |
| ORNL | | 4 (c) | | | | | | [21] |
| MIT | | | | 5 (d) | | | | [20] |
| Battelle | 2 (d) | | | | | | | [28] |
| Japanese | | | | 6 (b) | | | | [23, 26] |
| | | 12 (c) | | 12 (c) | | | | |
| HEDL | | | | | | | 11 (b) | [25] |
| GE | | | | | | 10 (a) | | [24] |
| Karlsruhe | | | | 7 (c) | | | | [2] |
| Cadarache | 3 (a) | | | | | | | [22] |

Table 2.
List of data analysed based on geometrical characteristics of bundle array.

| p/d | h/d | | | | | | | | | | | | |
|---|---|---|---|---|---|---|---|---|---|---|---|---|---|
| | 14 | 17 | 19 | 21 | 24 | 26.5 | 28 | 34 | 43 | 48 | 50 | 52 | 55 |
| 1.065 | | | 3* | | | | | | | | | | |
| 1.09 | | | | 12 | | | | | | | | | |
| 1.1 | | | | | | | | | | | | | |
| 1.14 | 3 | | | 3 | | | 3 | | | | | | |
| 1.20 | | | | | | | | | 6 | 1 | | | |
| | | | | | | | | | 12 | 8 | | | |
| 1.24 | | | | | | | | | | | | 4 | |
| | | | | | | | | | | 9 | | 11 | |
| 1.25 | | | | | 5 | | | | | 5 | | | |
| 1.28 | | | | | 10 | | | | | | | | 2 |
| 1.315 | | 7 | | | | | | 7 | | | 7 | | |
| 1.355 | | | | | | 3 | | | | | | | |

* Numbers refer to table 2.

was the coolant. An exit rake of thermocouples at the center of the subchannel was located 3 in. above the end of the heated zone (fig. 5). Flow enters the test bundle housing several inches below the heated zone. The container walls were surrounded by guard heaters to prevent radial heat loss. Several power skews, some as steep as 300% across the flats of the duct wall, were used in the test. The Reynolds number range was from 1000 to 70 000.

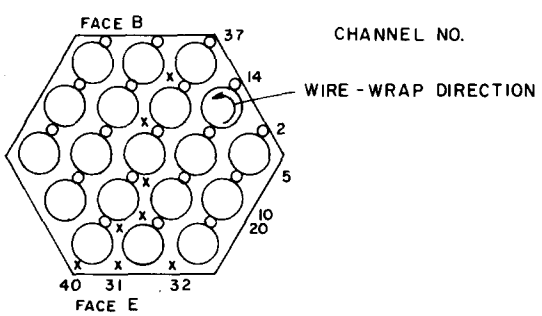


Fig. 5. Oak Ridge test bundle significant parameters. Test parameters [21] ! 1. Fluid-liquid Na. 2. Flow rate, up to 56 gpm (*Re* 1000–70 000). 3. Power skew: (a) all rods uniformly heated; (b) each rod heated individually; (c) B 20% higher than E; (d) E 20% higher than B; (e) B 300% higher than E; and (f) E 300% higher than B. 4. $d = 0.23$ in.; $h/d = 52$; and $p/d = 1.24$. $x \equiv$ location of exit thermocouple.

For the various test conditions of the ONRL data, eqs (3) and (4) were solved along with the boundary conditions. A single value of $\epsilon^*$ was assumed throughout the bundle.

For each of the test runs the best $\epsilon^*$ and $C$ was determined by choosing the magnitudes which gave a calculated fluid temperature distribution that agreed with the measured values (figs 6–9). Similar agreement was obtained for many others sets of the ONRL data.

In fig. 6 the magnitudes of $C$ and $\epsilon^*$ were varied. It is observed in fig. 6(a) that the magnitude selected for $\epsilon^*$ affects the agreement everywhere, but fig. 6(b) illustrates that the magnitude of $C$ affects the agreement only at the positions near the outer edges (region II) of the core. Therefore, $\epsilon^*$ is determined first by obtaining agreement in the inner region.

The magnitude of $\epsilon^*$ is plotted versus Reynolds number in fig. 10. The Reynolds number in fig. 10 is defined

$$Re = [\rho(\bar{U}/\bar{\lambda}_a)d_e]/\mu.$$

Since $\bar{U}$ is the superficial bundle average velocity, the ratio $\bar{U}/\bar{\lambda}_a$ gives the actual average bundle velocity in the free space. $\bar{\lambda}_a$ is defined as the bundle average void area per unit total area, and is uniform for all axial levels. It is observed that $\epsilon^*$ is essentially constant over the design range of Reynolds number of present reac-

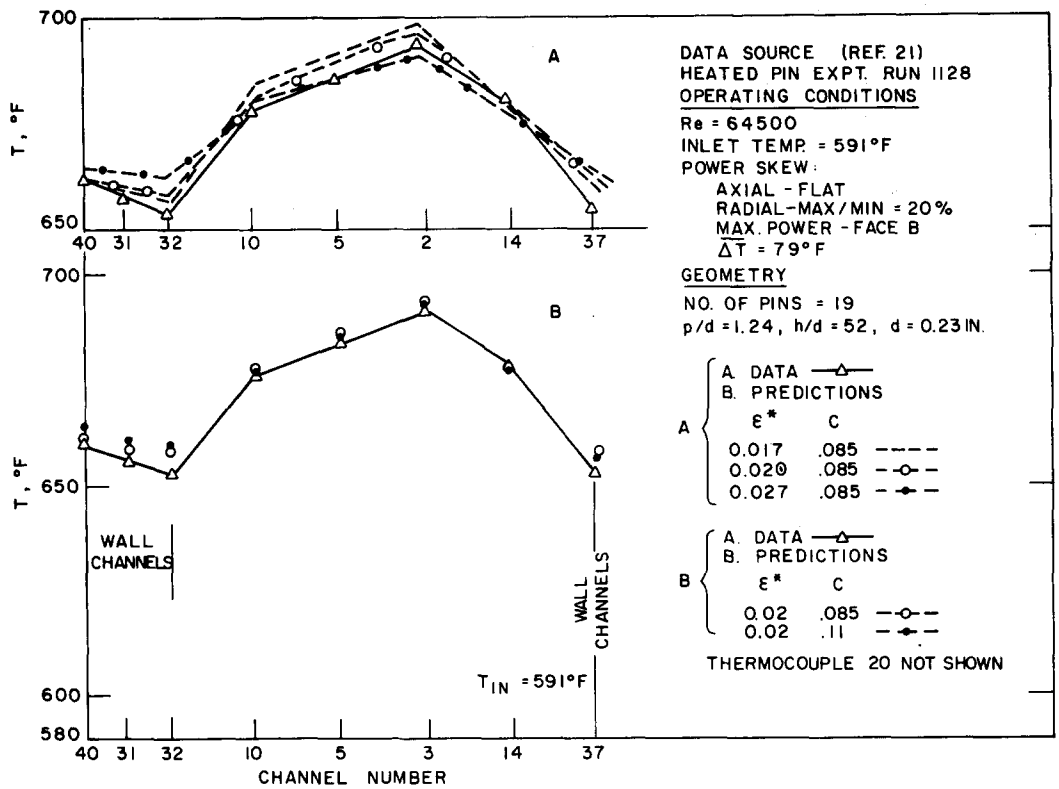


Fig. 6. Parametric study of determining $\epsilon^*$ and $C$.

tor fuel assemblies: 15 000–70 000. It was found that $C = 0.069$ resulted in best agreement between experimental and analytical results for the wire pitch-to-diameter ratio of 52.

Comparison of these results with other predictive methods [4, 9] being currently used in LMFBR design, have been made. Figs 8 and 9 show that this method predicts temperature distribution at the exit of the ORNL fuel assembly to the same degree of accuracy. These other methods, codes COTEC [4] and THI-3D [9], were also calibrated with a portion of the ORNL data before predictions of the rest of data were made.

Figures 11 and 12 show the dependence of $\epsilon^*$ and $C$ on $h/d$ and $p/d$. For each set of data analysed, no dependence of $\epsilon^*$ and $C$ on Reynolds number was found for Reynolds numbers $\geqslant 9000$. The effect of Prandtl number is also very small, because the predominant mixing process in wire-wrapped bundles operating at high Reynolds number is not of the boundary layer mixing type but a bulk mixing process. This is also clear from the fact that the enhanced eddy diffusivity $\epsilon^*$ which models the bulk mixing here is an order of magnitude larger than $\kappa\alpha^*$ for the high Reynolds number ($Re \geqslant 9000$) range of operating of fuel assemblies. However, at low Reynolds numbers, when $\kappa\alpha^*$ is of the same magnitude as $\epsilon^*$, the effect of Prandtl number on $\epsilon^*$ and $C$ would be more important.

A correlation was obtained from figs 11 and 12 for $\epsilon^* = f(h/d, p/d)$ and $C = f(h/d)$. The effect of $p/d$ on $C$ was found to be very small and therefore it was not included. These correlations can be built directly into the ENERGY code, but must be used only for bundles in forced convection and with the following additional restrictions:

(a) all wire wraps are of the same diameter wrapped in the same sense from the same start position;

(b) $14 \leqslant h/d \leqslant 52$; and

(c) $1.14 \leqslant p/d \leqslant 1.32$.

The correlations for $\epsilon^*$ and $C$ are as follows:

$$\epsilon^* = [0.85 - 12.8\,\{|p/d - 1.25|\}^{1.424}]\,(d/h), \quad (9)$$

$$C = 0.09 + 2(d/h - 0.03). \quad (10)$$

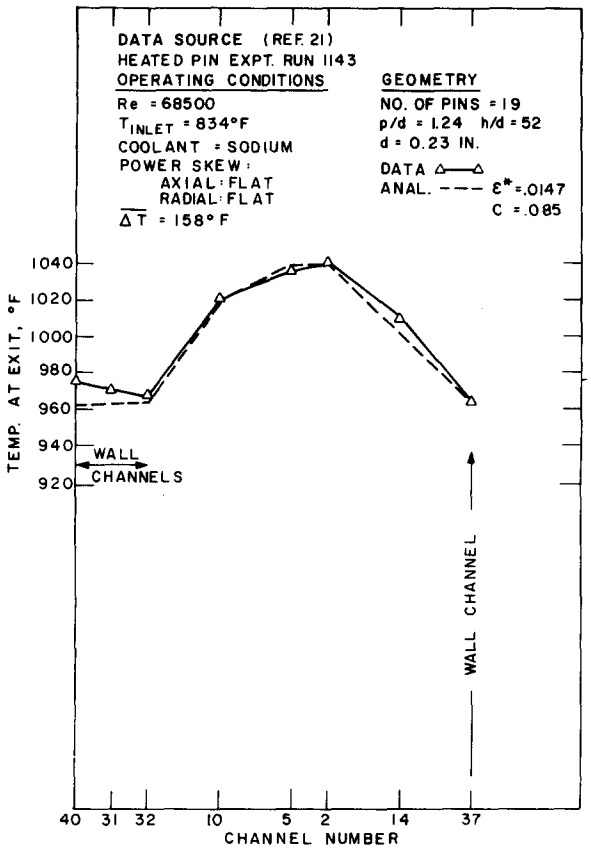


Fig. 7. Exit temperature distribution for uniform power.

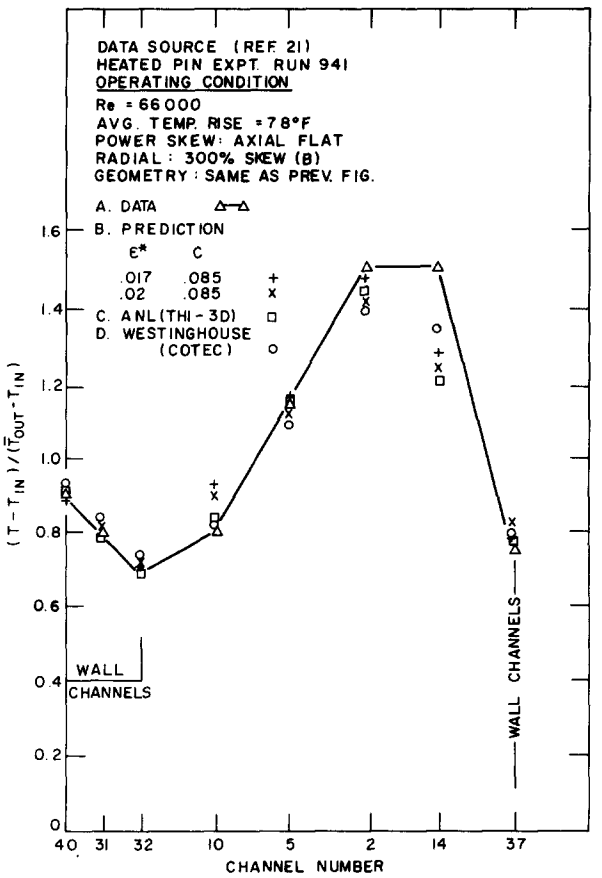


Fig. 8. Comparison of exit temperatures for 300% skew (B).

The correlation for $\epsilon^*$ is considered good within ±20% at the 95% confidence level and the correlation for $C$ is good within ±35% at the 95% confidence level.

A few data points (fig. 12) lie above the line representing the tangent of the wire wrap angle, which we may expect to be the upper limit of $C$. It is possible that the discrepancy may be attributed to the error associated with each set of data. Only a few error bars are shown in fig. 12 in order to maintain clarity. Although the mean value lies above the line representing the tangent of the wire wrap angle, the error bars extend to points well below it.

The correlation for $C$, eq. (10), however, lies below the tangent of the wire-wrap angle in the entire design range of $d/h$ for fuel and blanket assemblies. Since the circumferential temperatures are relatively insensitive to $C$, the large error bars should not be of serious concern.

## 5. Conclusion

A simplified method based on a model analogous to that for heat transfer in a porous body has been developed for predicting temperature distributions in wire-wrapped LMFBR fuel rod bundles. The results obtained match the available data with the same precision as more complicated subchannel analysis codes. Correlations for the two empirical constants which appear in this model were obtained as a function of the geometrical parameter of a fuel assembly. With these correlations, this method can predict temperature distributions in any fuel assembly whose geometry is within the limits of the parameters for which correlations for $\epsilon^*$ and $C$ were obtained. This, along with the short computational time (20 sec for a 217-pin bundle calculation on IBM-360), make this model a useful design tool.

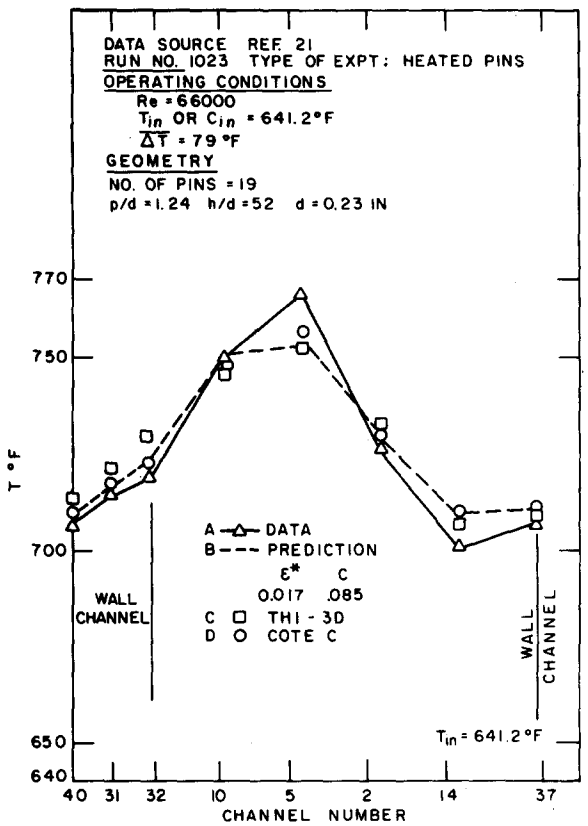


Fig. 9. Comparison of experimental and analysis exit temperatures, 300% skew (E).

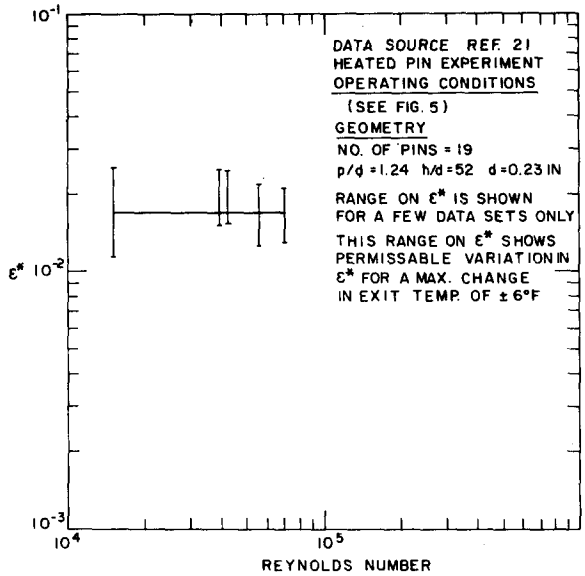


Fig. 10. Variation of $\epsilon^*$ versus Reynolds number.

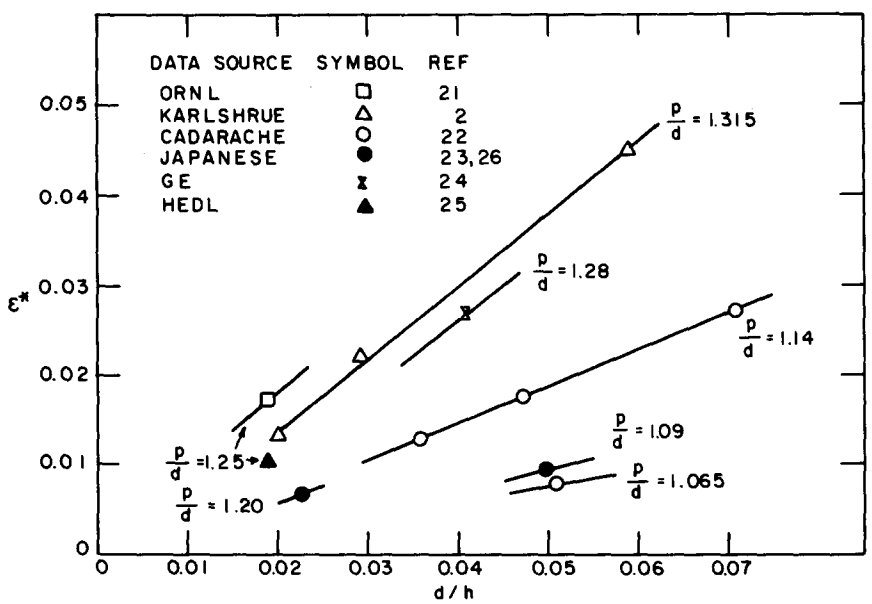


Fig. 11. Variation of $\epsilon^*$ versus $(d/h)$ for various values of $p/d$.

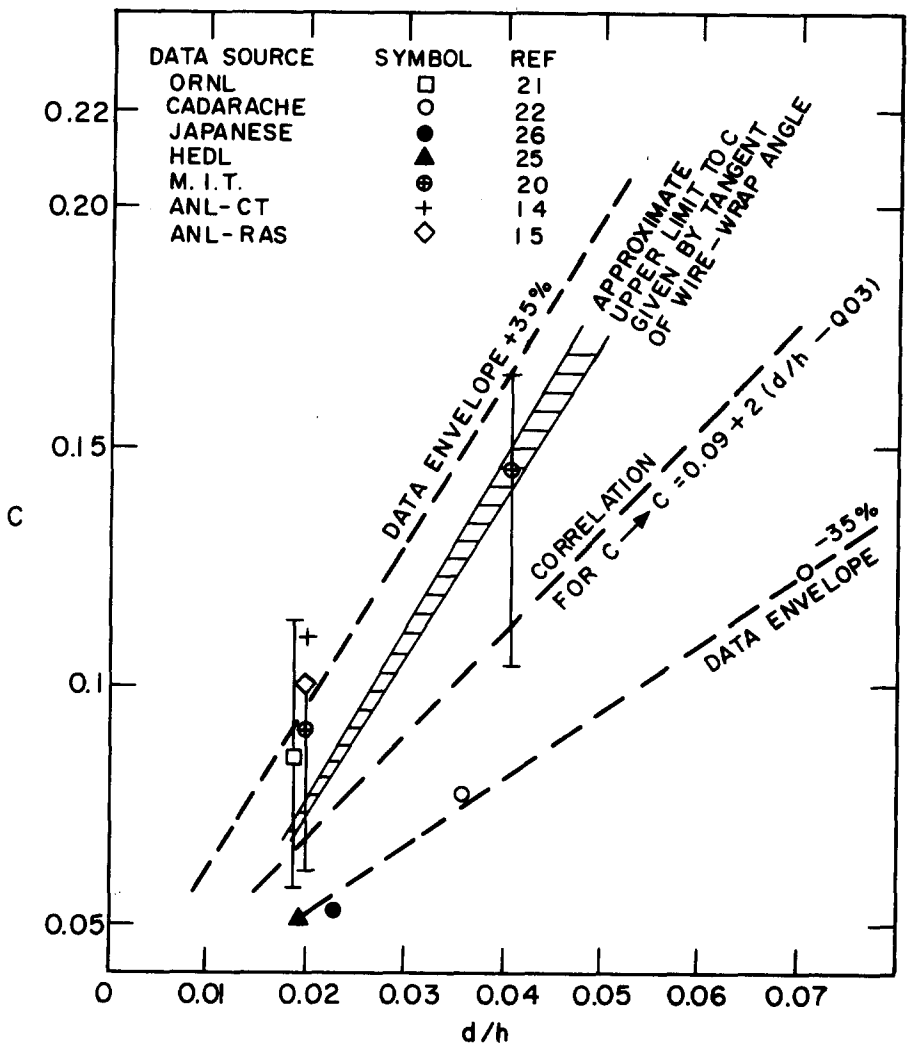


Fig. 12. Variation of $C$ with $d/h$.

**Nomenclature**

| | |
|---|---|
| $C$ | = ratio of superficial swirl velocity to bundle average velocity (= $U_s/\bar{U}$) |
| $C_p$ | = specific heat |
| $d_e$ | = hydraulic diameter of an actual interior channel |
| $dw$ | = wire-wrap diameter |
| $d$ | = rod diameter |
| $f$ | = friction factor |
| $h$ | = wire-wrap lead |
| $h^*$ | = dimensionless enthalpy used only in eq. (4) for ENERGY-I formulation |
| $K$ | = thermal conductivity |
| $L$ | = length of bundle |
| $n$ | = coordinate in region II perpendicular to wall |
| $n^*$ | = dimensionless coordinate |
| $Pr$ | = Prandtl number |
| $P$ | = pressure |
| $Q$ | = heat generation per unit (total) volume at the point $x, y, z$ |
| $Q^*$ | = dimensionless heat generation (= $Q/\bar{Q}$) |
| $\bar{Q}$ | = average heat generation per unit (total) volume |
| $Re$ | = Reynolds number (= $Gd_e/\mu$) |
| $s$ | = coordinate in region II parallel to duct wall |

$s^*$ = dimensionless coordinate
$T$ = coolant temperature at the point $x, y, z$ in the bundle
$\bar{T}$ = average coolant temperature in the cross section of the bundle
$T_M$ = average exit coolant temperature
$T_{IN}$ = inlet coolant temperature
$t$ = thickness of region II
$(U_I)_z$ = superficial axial velocity in region I
$(U_{II})_z$ = superficial axial velocity in region II
$\bar{U}$ = bundle average superficial velocity
$U_s$ = superficial swirl velocity in region II

*Greek symbols*

$\epsilon$ = effective enhanced eddy diffusivity
$\epsilon^*$ = dimensionless eddy diffusivity $(= \epsilon/\bar{U}d_e)$
$\alpha$ = thermal diffusivity
$\alpha^*$ = dimensionless thermal diffusivity $(= \alpha/\bar{U}d_e)$
$\kappa$ = constant for two-dimensional transverse heat flow in porous media
$\rho$ = density
$\mu$ = viscosity
$\gamma$ = kinematic viscosity
$\eta_T$ = node spacing in region I
$\eta_T^*$ = dimensionless node spacing in region I $(= \eta T/d_e)$
$\eta_s$ = node spacing in $s$ direction in region II
$\eta_s^*$ = dimensionless $\eta_s$
$\eta_n$ = node spacing in $n$ direction in region II
$\eta_n^*$ = dimensionless $\eta_n$

*Subscripts and superscripts*

$*$ = dimensionless number
$s$ = coordinate parallel to duct wall
$n$ = coordinate perpendicular to duct wall
IN = inlet to bundle
I = region I
II = region II.

## References


[1] E. Khan, W. Rohsenow, A. Sonin and N. Todreas, A simplified approach for predicting temperature distribution in wire-wrapped assemblies, Topical Report, COO-2245-5TR, Sept. (1973).

[2] H. Hoffman and E. Bumgartner, Experimental investigations of the thermodynamic behavior of fast breeder reactor fuel element with different spacer types, Fuel Elements for Fast Reactors, vol. I, IAEA, Vienna (1974).

[3] C. Wheeler, COBRA-IIA – A program for thermal hydraulic analysis in very large bundles of fuel pins, BNWL-1422, Aug. (1970).

[4] E. Novendstern, Mixing model for wire-wrap fuel assemblies, Trans. ANS 15 (2), Nov. (1972).

[5] A.W. Graves and Ivan Catton, A numerical model for heat transfer in rod bundle with helical wire wrap spacers, ASME, Paper 72-T-55, Aug. (1972).

[6] P.M. Magee, Modeling of flow sweeping effect in wire-wrapped rod Bundles, Trans. ANS 15 (1), June (1972).

[7] J.L. Wantland, ORRIBLE – A computer program for flow and temperature distribution in LMFBR fuel rod assemblies, ORNL, TM-3516, Oct. (1971).

[8] D.S. Rowe, COBRA IIIC – A digital computer program for steady state and transient thermal hydraulic analysis rod bundle nuclear fuel element, BNWL-1695, Mar. (1973).

[9] W.T. Sha, R.C. Schmitt and P.R. Huebotter, Temperature mapping of CRBRP blanket assembly using the THI-3D computer program, Trans. ANS 19, Oct. (1974) 324–325.

[10] R.A. Bernard and R.H. Wilhelm, Turbulent diffusion in fixed beds of packed solids, Chem. Eng. Progr. 46 (5) (1950). 233.

[11] T.A. Baron, Generalized graphical method for the design of fixed bed catalytic reactors, Chem. Eng. Progr. 48 (3) (1952) 118.

[12] D.A. Plantz and H.F. Johnstone, Heat and mass transfer in packed beds, AIChE J. (2) (1955) 193.

[13] G.S.G. Beveridge and D.P. Haroglíey, Axial heat transfer in packed beds, Int. J. Heat Mass Transfer 14 (1971) 1093.

[14] J.J. Lorenz, T. Ginsberg and R.A. Morris, Experimental mixing studies and velocity measurements with a simulated 91-element LMFBR fuel assembly, ANL-CT-74-09, Argonne National Laboratory, Feb. (1974).

[15] D.R. Pederson, R.D. Pierce, R.E. Wilson and C.J. Roop, Cross-flow mixing in a 91-element bundle, ANL/RAS 74-2, Argonne National Laboratory, Feb. (1974).

[16] E.H. Novendstern, Turbulent flow pressure drop model for fuel rod assemblies utilizing a helical wire-wrap spacer system, Nucl. Eng. Des. 22 (1) Aug. (1972).

[17] E. Khan, N. Todreas, W.M. Rohsenow and A.A. Sonin, Analysis of mixing data relevent to wire-wrapped fuel assembly thermal-hydraulic design, COO-2245-12, Topical Report, MIT, Sept. (1974).

[18] W.M. Rohsenow and H.Y. Choi, Heat Mass and Momentum Transfer, 3rd edn, Prentice-Hall, New Jersey (1961).

[19] A.E. Scheidegger, The Physics of Flow Through Porous Media, University of Toronto Press (1960).

[20] Y.B. Chen, K. Ip and N.E. Todreas, Velocity measurement in edge subchannels of wire wrapped LMFBR fuel assemblies, COO-2245-11TR, MIT, Sept. (1974).

[21] M.H. Fontana et al., Temperature distribution in the duct

wall and at the exit of a 19-rod simulated LMFBR fuel assembly (FFM-2A), ORNL-4852, Apr. (1973).
[22] J. Skok, Mixing of the fluid due to helecoidal wires of fuel pins in a triangular array, Progress in Heat and Mass Transfer, vol. 7 (1973).
[23] Y. Okamoto, N. Akuno, K. Enion and M. Tanuda, Hydraulic tests on FBR fuel sub-assemblies, JAPFNR-24 (1970).
[24] D.P. Hines, L.R. Boyd and V.R. Marian, In-core-boiling or over temperature detector development, General Electric, NEDO-13650, Apr. (1971).
[25] R.E. Collingham, W.L. Thorne and J.D. McCormack, 217 pin wire wrapped bundle coolant mixing test, MEDL-TME 71-146, Nov. (1971).
[26] E. Ishibashi, Some topics of sodium technology research and development in PNC Japan, Report of the O-ARAI Engineering Center, Power Reactor and Nuclear Fuel Development Corporation, Japan.
[27] J.J. Lorenz and T. Ginsberg, Results and analysis of 7 pin wire wrap mixing tests, Trans. ANS 15 (2) 1972.
[28] C.L. Wheeler, D.S. Rowe and J. Smith, An experimental study of axial and cross flow bundle, BNWL-1804, Feb. (1974).
[29] E.U. Khan, A porous body model for predicting temperature distributions in wire wrapped fuel and blanket assemblies of a liquid metal fast breeder reactor, Sc.D. Thesis, Department of Mechanical Engineering, MIT, Cambridge, Mass., Jan. (1975).